# "Ependymal-in" Gradient of Thalamic Damage in Progressive Multiple Sclerosis

Roberta Magliozzi, PhD [1,2‡] Giulia Fadda, MD, PhD [3‡] Robert A. Brown, PhD,[4‡]
Amit Bar-Or, MD, PhD,[3] Owain W. Howell, PhD [2,5] Simon Hametner, MD, PhD,[6]
Damiano Marastoni, MD,[1] Alberto Poli, MD,[1] Richard Nicholas, MD, PhD [2]
Massimiliano Calabrese, MD,[1†] Salvatore Monaco, MD, PhD,[1†] and
Richard Reynolds, PhD[2,7†]

Leptomeningeal and perivenular infiltrates are important contributors to cortical grey matter damage and disease progression in multiple sclerosis (MS). Whereas perivenular inflammation induces vasculocentric lesions, leptomeningeal involvement follows a subpial "surface-in" gradient. To determine whether similar gradient of damage occurs in deep grey matter nuclei, we examined the dorsomedial thalamic nuclei and cerebrospinal fluid (CSF) samples from 41 postmortem secondary progressive MS cases compared with 5 non-neurological controls and 12 controls with other neurological diseases. CSF/ependyma-oriented gradient of reduction in NeuN$^+$ neuron density was present in MS thalamic lesions compared to controls, greatest (26%) in subventricular locations at the ependyma/CSF boundary and least with increasing distance (12% at 10 mm). Concomitant graded reduction in SMI31$^+$ axon density was observed, greatest (38%) at 2 mm from the ependyma/CSF boundary and least at 10 mm (13%). Conversely, gradient of major histocompatibility complex (MHC)-II$^+$ microglia density increased by over 50% at 2 mm at the ependyma/CSF boundary and only by 15% at 10 mm and this gradient inversely correlated with the neuronal ($R = -0.91$, $p < 0.0001$) and axonal ($R = -0.79$, $p < 0.0001$) thalamic changes. Observed gradients were also detected in normal-appearing thalamus and were associated with rapid/severe disease progression; presence of leptomeningeal tertiary lymphoid-like structures; large subependymal infiltrates, enriched in CD20$^+$ B cells and occasionally containing CXCL13$^+$ CD35$^+$ follicular dendritic cells; and high CSF protein expression of a complex pattern of soluble inflammatory/neurodegeneration factors, including chitinase-3-like-1, TNFR1, parvalbumin, neurofilament-light-chains and TNF. Substantial "ependymal-in" gradient of pathological cell alterations, accompanied by presence of intrathecal inflammation, compartmentalized either in subependymal lymphoid perivascular infiltrates or in CSF, may play a key role in MS progression.

**Summary for Social Media:** Imaging and neuropathological evidences demonstrated the unique feature of "surface-in" gradient of damage in multiple sclerosis (MS) since early pediatric stages, often associated with more severe brain atrophy and disease progression. In particular, increased inflammation in the cerebral meninges has been shown to be strictly associated with an MS-specific gradient of neuronal, astrocyte, and oligodendrocyte loss accompanied by microglial activation in subpial cortical layers, which is not directly related to demyelination.

To determine whether a similar gradient of damage occurs in deep grey matter nuclei, we examined the potential neuronal and microglia alterations in the dorsomedial thalamic nuclei from postmortem secondary progressive MS cases in

combination with detailed neuropathological characterization of the inflammatory features and protein profiling of paired CSF samples.

We observed a substantial "subependymal-in" gradient of neuro-axonal loss and microglia activation in active thalamic lesions of progressive MS cases, in particular in the presence of increased leptomeningeal and cerebrospinal fluid (CSF) inflammation. This altered graded pathology was found associated with more severe and rapid progressive MS and increased inflammatory degree either in large perivascular subependymal infiltrates, enriched in B cells, or within the paired CSF, in particular with elevated levels of a complex pattern of soluble inflammatory and neurodegeneration factors, including chitinase 3-like-1, TNFR1, parvalbumin, neurofilament light-chains and TNF.

These data support a key role for chronic, intrathecally compartmentalized inflammation in specific disease endophenotypes. CSF biomarkers, together with advance imaging tools, may therefore help to improve not only the disease diagnosis but also the early identification of specific MS subgroups that would benefit of more personalized treatments.

Cortical grey matter (GM) and deep GM (DGM) tissue damage in multiple sclerosis (MS) exhibits significant pathological differences when compared to white matter (WM) lesions, such as a relative paucity of parenchymal inflammatory cells and a prevailing pattern of damage that follows a surface-in gradient, rather than the typical perivascular distribution of focal WM lesions.[1–3] Neuropathological studies demonstrate a close association between the degree of meningeal inflammation and the severity of subpial cortical damage.[3–6] In particular, increased inflammation in the cerebral meninges has been shown to be strictly associated with a gradient of neuronal, astrocyte, and oligodendrocyte loss accompanied by microglial activation in subpial cortical layers, which is not directly related to demyelination. Neuronal and glial alterations are greatest in the most external cortical layers (I–III) and decrease in the most innermost ones closest to the WM.[3]

Recent combined molecular neuropathology studies on progressive MS cases at postmortem and imaging and cerebrospinal fluid (CSF) analysis in patients with newly diagnosed MS has demonstrated that common intrathecal (meninges and CSF) inflammatory profiles are linked to increased cortical pathology, both at the time of the diagnosis and at death.[5–7] These results raised the hypothesis that soluble factors produced by meningeal inflammatory cells and/or immune cells circulating in the CSF may be released into the CSF and may diffuse into the GM contributing to graded pathological changes, including demyelination, microglial activation, and neuronal loss.[8–15] This increased inflammation in the subarachnoid space is also associated with increased gene expression for TNF/TNF receptor 1-mediated cell death signaling pathways in the cortical GM of postmortem brains with meningeal tertiary lymphoid-like structures (TLS).[16] In support of these findings, advanced 7 Tesla magnetic resonance imaging (MRI) methodology has shown the presence of a gradient of subpial cortical alterations,[3,17–20] and, in addition, the presence of "outside-in" graded abnormalities in all brain surfaces exposed to CSF has been shown using either magnetization transfer ratio (MTR) or diffusion tensor imaging (DTI).[17–20]

Several other findings suggest that the mechanisms underlying these progressive changes may manifest early, rather than starting late in the disease course.[21–24] The idea that a gradient of injury is an early pathological event in MS is supported by the recent finding of a "surface-in" gradient of thalamic damage already notable in the first year of clinical disease in pediatric MS, which worsened over time.[23,24] This finding was specific for children with MS, as it was not observed in healthy controls or children with monophasic demyelination.

Thalamic pathology, in particular substantial neuronal loss (30–35% reduction), was an early and prominent involvement in MS.[23–25] The current study aimed to determine whether a gradient of inflammatory and neurodegenerative tissue pathology, similar to the one previously detected in the motor cortex and linked to meningeal inflammation, can be observed in the thalamus, which has a CSF-interface on the ventricular side. Furthermore, we evaluated any possible correlation between graded thalamic injury and CSF inflammatory profile.

## Methods

### Postmortem Tissue Sampling

One paraffin embedded 4% paraformaldehyde-fixed block (2 cm × 2 cm) containing the dorsomedial nucleus of the thalamus (block number 8 obtained at the time of brain dissection from the subthalamic nucleus, Fig 1A, B) was examined from each of 41 postmortem MS brains (mean age = 58.48 ± 14.83 years; Table S1) and 5 non-neurological controls (mean age = 62.6 ± 17.18). Tissues were obtained from the UK Multiple Sclerosis Society Tissue Bank (UKMSTB) at Imperial College, under ethical approval (08/MRE09/31). The diagnosis of MS was confirmed by neuropathology according to the International Classification of Diseases of the Nervous System
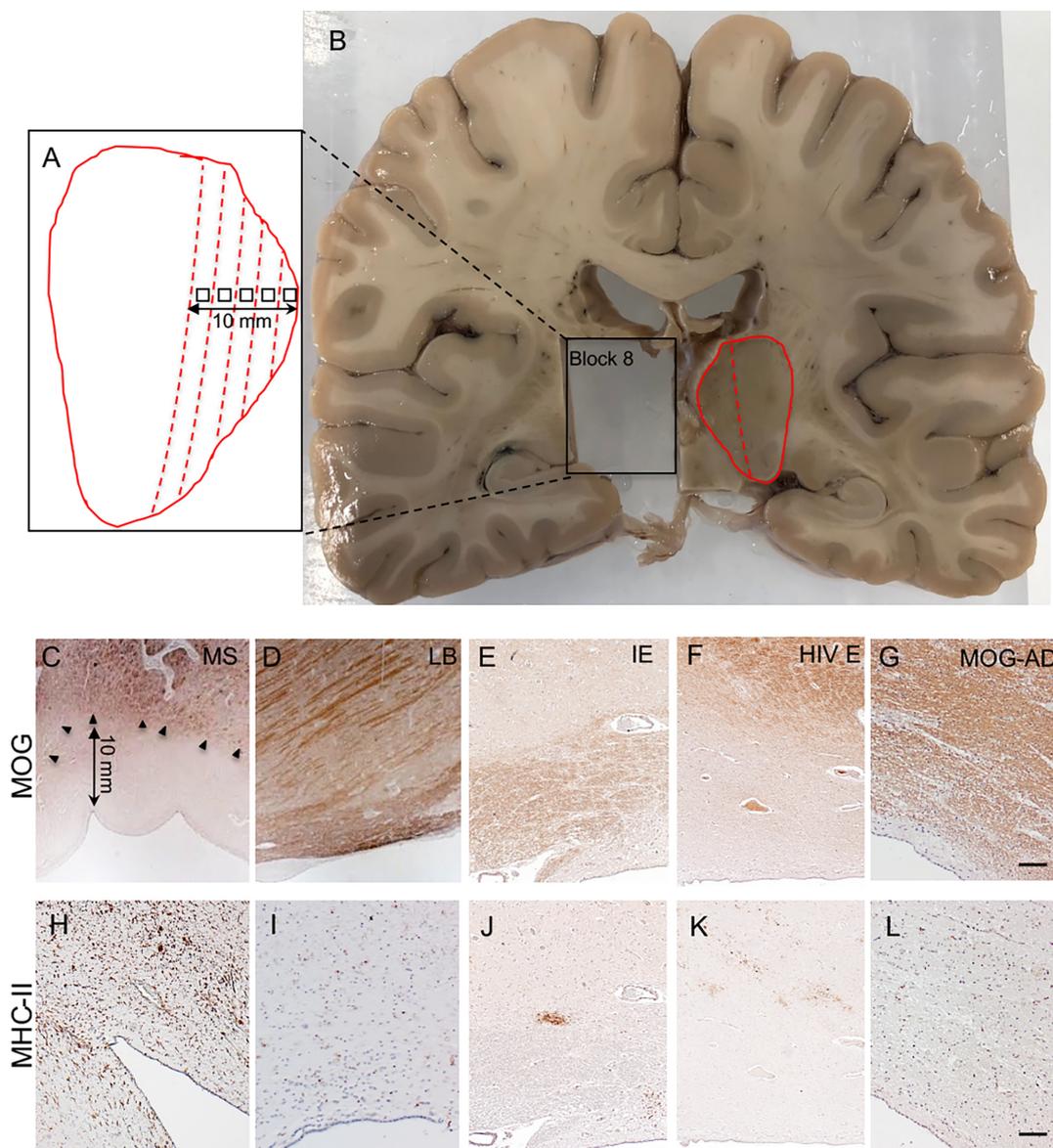
FIGURE 1: Schematic illustration of the thalamic tissue block examined from postmortem MS and control cases and of the thalamic area examined for cell density according to the adjacent layers within a 10 mm-distance from the CSF/ependymal boundary (A). Immunohistochemistry detection of myelin oligodendrocyte glycoprotein (MOG) and of the major histocompatibility complex class II molecules (MHC-II) on serial sections of postmortem thalamic tissues from patients with MS (C), Lewy body dementia (D), ischemic encephalopathy (E), HIV encephalitis (F), MOG antibody mediated disease (G). Subependymal demyelination (underlined by arrowheads) was evident in MS cases (C) but not in the other neurological controls (D–G). Parallel increased density of MHC-II$^+$ microglia/macrophages close to the CSF/ependyma boundary in MS cases with active thalamic demyelination (H) but not in the other examined neurological conditions (I–L). Only rare and scattered MHC-II$^+$ activated microglial cells were identified in other inflammatory neurological disease thalamic tissue samples in the subependymal area, with the majority of microglia/macrophages detected as discreet foci adjacent to parenchymal vessels (Fig 1J–L). Scale bar: 1000 μm (C–L). CSF = cerebrospinal fluid; H&E = hematoxylin and eosin stain; NAT = normal appearing thalamus; TL = thalamic lesion; TLS = lymphoid-like structure.

criteria (www.ICDNS.org). In addition, 12 age-matched controls with other neurological diseases have been included: (1) 4 controls with other noninflammatory neurodegenerative conditions (2 with Parkinson's disease, 1 with Lewy body dementia, and 1 with Alzheimer's disease) were obtained from the Neurology unit of University of Verona (ethical approval 140,173, 05/06/2017); (2) 3

controls with other inflammatory diseases (1 case of ischemic encephalopathy, 1 case of cytomegalovirus encephalitis, and 1 case of HIV encephalitis), were obtained from the Oxford Brain Bank, supported by the Medical Research Council, Brains for Dementia Research (Alzheimer Society and Alzheimer Research UK), under research ethics committee approval (South West Wales REC #13/WA/0292; see

Table S1); (3) 5 cases with other inflammatory diseases (1 case with neuromyelitis optica [NMO], 1 case with NMO spectrum disorder [NMOSD] + myelin oligodendrocyte glycoprotein-antibody-associated disease [MOGAD], 2 cases with MOGAD, and 1 case of acute purulent meningoencephalitis) were obtained from the Medical University of Vienna (approved by the institutional review board of the Medical University of Vienna, EK #1123/2015). All the available demographic and clinical data of MS and control cases are reported in Table S1.

### Immunohistochemistry/Immunofluorescence

Serial paraffin sections (7 μm) were de-waxed and rehydrated in phosphate buffered saline (PBS). Immunohistochemistry and immunofluorescence detection of the examined antibodies indicated in Table 1 was performed according to the procedures previously optimized.[3–7] Negative controls were included in each experiment and all sections from all cases were stained together in the same experimental run. The presence and classification of the demyelinating activity of each thalamic lesion (TL) was assessed by immunohistochemical detection of myelin oligodendrocyte glycoprotein (MOG) in combination with the major histocompatibility complex (MHC) class II on serial sections, as previously described[3–5]: active lesions contained numerous MHC class II$^+$ cells both in the lesion core and at the lesion border; chronic active lesions had mainly a border of MHC class II$^+$ cells and a lower number in the core; chronic inactive lesions had a very low MHC class II$^+$ cell density throughout the lesion. All sections were counterstained with hematoxylin, sealed with Entellan rapid mounting medium, and viewed with a ZEISS Axioscope microscope (ZEISS International, Germany). Images were captured with a Axiocam 208 Colorcamera (ZEISS).

### Cell Count and Morphometric Analysis

Cell (neurons and microglia) density and morphometric analysis was performed in 20 out of 41 MS cases, by selecting the 10 MS cases previously characterized for the presence of meningeal TLS$^+$ (age at onset = 27.1 ± 4.3 years, age at death = 45.4 ± 7.3 years; see Table S1) and 10 MS cases without meningeal TLS (TLS$^-$; age at onset = 30.4 ± 6.9 years, age at death = 55.7 ± 9.7 years; see Table S1). These 20 selected MS cases represent the same MS cohort previously characterized for the presence of a substantial subpial gradient of cell and/or molecular alterations in the corresponding motor cortex as well as for the specific CSF protein profile.[3–5,7,16] For each of the 20 MS cases and of 5 non-neurological controls one paraffin embedded 4% paraformaldehyde-fixed block (2 cm × 2 cm) containing the dorsomedial nucleus of the thalamus (see Fig 1A, B) was examined. The numerical density of NeuN$^+$ neurons and

MHC-II$^+$ microglia/macrophages was determined in both TLs (characterized as active or chronic active lesions) and in areas of normal appearing thalamus (NAT) of 10 TLS MS cases (see Table S1), 10 TLS$^+$ MS cases (see Table S1), and in the 5 non-neurological controls, using previously described optimized protocols[3,26] (see Figs 1, 2). In addition, the number of SMI31$^+$ axons was counted using a morphometric grid (number of immunoreactive axons/mm$^2$). Briefly, 5 consecutive fields of view (20× objective; ZEISS Axioscope microscope equipped with an Axiocam 208 Color-camera), moving from the CSF-thalamic interface toward the internal capsule for a distance of 10 mm from the CSF/ependyma boundary, were captured, coded for blinding with respect to case and pathology and quantified (see Fig 1A). Cells were manually counted in a rectangular grid located away from the edges of the field to avoid double counting between adjacent fields (see Fig 1A). Counts were repeated on 3 serial sections for each immunostaining for each MS and control case within the same experiment (in all cases blinded to diagnosis and myelin status). Mean cell counts measured in MS TL and NAT were normalized to the mean values of the corresponding fields in the non-neurological controls and expressed as percentage change. In addition, the "f-circle" function was used as a measure of neuronal shape changes: increasing f-circle values correspond to objects that are increasingly circular rather than elliptical.[27] Briefly, serial sections were immunostained with the neuronal marker microtubule-associated protein 2 (MAP2) and the same 5 consecutive fields of view used for neuronal cell count (20× objective) were captured. Neuronal area and perimeter were measured by using open-source software for digital pathology image analysis (QuPath) in order to quantify the f-circle, calculated as 4p (area/perimeter$^2$).

### Qualitative and Quantitative Analysis of Parenchymal and Perivascular Inflammation

Total microglial/macrophage numbers were evaluated using antibodies to MHC-class II$^+$ antigen, together with TMEM119 for the resident homeostatic microglia, CD68 for activated phagocytic microglia/macrophages, CD11c as a marker of antigen presentation by activated microglia/macrophages, CD86 as evidence of co-stimulatory activity and CD163 as a surface marker of alternative microglial/macrophage activation.[28]

The presence of CD3$^+$ T- and CD20$^+$ B-cells, plasma cells, as well as follicular dendritic markers (CD35$^+$) and of the B-cell chemoattractant chemokine CXCL13, was evaluated in the tissue parenchyma and in subependymal perivascular infiltrates of the active TL, following previously optimized immunohistochemistry and immunofluorescence procedures.[4,5] All sections used for immunofluorescence were counterstained with DAPI

## TABLE 1. Primary Antibodies Used for Immunohistochemistry/Immunofluorescence

| Antigen | Specificity | Clone | Dilution | Source |
|---|---|---|---|---|
| MOG[c] | Myelin oligodendrocyte glycoprotein | Z12 | 1:50 | In house, R. Reynolds, Imperial College, London, UK |
| MHC class II | Antigen presenting cells | CR3/43 | 1:50 | Dako, Carpinteria, CA, USA |
| NeuN | Neuronal nuclei | Rabbit polyclonal | 1:1000 | Millipore/Merck, Merck KGaA, Darmstadt, Germany |
| MAP2 | Microtubule-associated protein 2 | Rabbit polyclonal | 1:200 | Dako |
| SMI31 | Neurofilament heavy polypeptide | Mouse | 1:200 | BioLegend, San Diego, CA USA |
| CD68 | Activated microglia/macrophages | KP1 | 1:50 | Dako |
| TMEM119 | Transmembrane protein 119 | Rabbit polyclonal | 1:100 | Sigma-Aldrich, Burlington, MA, USA |
| CD86 | Co-stimulatory T cell signal | Goat polyclonal | 1:100 | R&D Systems, Minneapolis, MN, USA |
| CD163 | Hemoglobin-haptoglobin scavenger receptor | 10D6 | 1:500 | Novocastra, Leica Biosystem, Wetzlar, Germany |
| CD11c | Integrin alpha X (ITGAX) | KB90 | 1:50 | Dako |
| CD3[a] | T lymphocytes | EP449E | 1:125 | ThermoFisher, Waltham, MA, USA |
| CD20[a] | B lymphocytes | L26 | 1:250 | ThermoFisher |
| CD35[b] | Follicular dendritic cells | Ber/MAC/DRC | 1:50 | Dako |
| CXCL13[b] | CXCL13/BCA1 chemokine | Goat polyclonal | 1:50 | R&D System |
| Fluorescein-conjugated Ig-A,-G, −M | Plasma cells/plasma blasts | Rabbit polyclonal | 1:500 | Dako |

Antigen retrieval procedures used in this study:

[a]30 min in steamer in sodium citrate buffer pH 6.

[b]30 min in steamer in Dako target retrieval solution pH 9.

[c]Permeabilization with cold methanol.

MHC = major histocompatibility complex; MOG = myelin oligodendrocyte glycoprotein.

and viewed with a Leica THUNDER Imager Tissue microscope (Leica Microsystem, Germany). In addition, counts of CD3$^+$ T cells and CD20$^+$ B cells were performed for each perivascular infiltrate found in close proximity to the ependymal surface: only large perivenular spaces, with a diameter of 200 to 500 μm, in close proximity to the ependyma were selected. For each TLS$^+$ and TLS$^-$ case one subependymal infiltrate was selected and the CD3$^+$ and CD20$^+$ lymphocyte counts were manually performed in consecutive paraffin sections. All the antibodies used are listed in Table 1.

### Postmortem CSF Protein Analysis

The levels of 89 inflammatory mediators were determined in the paired CSF samples of each TLS$^+$ and TLS$^-$ case, using custom immune-assay multiplex Luminex technology (Bio-Plex X200 System equipped with a magnetic workstation; BioRad, Hercules, CA), following the procedures previously optimized.[7] The levels of neurofilament light-chain proteins were measured using the Human NF-light enzyme-linked immunosorbent assay (ELISA) kit (MyBioSource, San Diego, CA) according to the procedures previously optimized.[7] In addition, the protein levels of CSF fibrinogen total antigen (#MBS135523; MyBiosource) were measured by ELISA assay, as previously optimized.[29] Finally, the CSF protein levels of parvalbumin (PVALB), a protein specifically expressed by GABAergic interneurons, which is a marker of cortical GABA-ergic interneurons in patients with MS with more severe disease course,[29] was measured by ELISA assay (MBS2022353; MyBioSource) according to previously
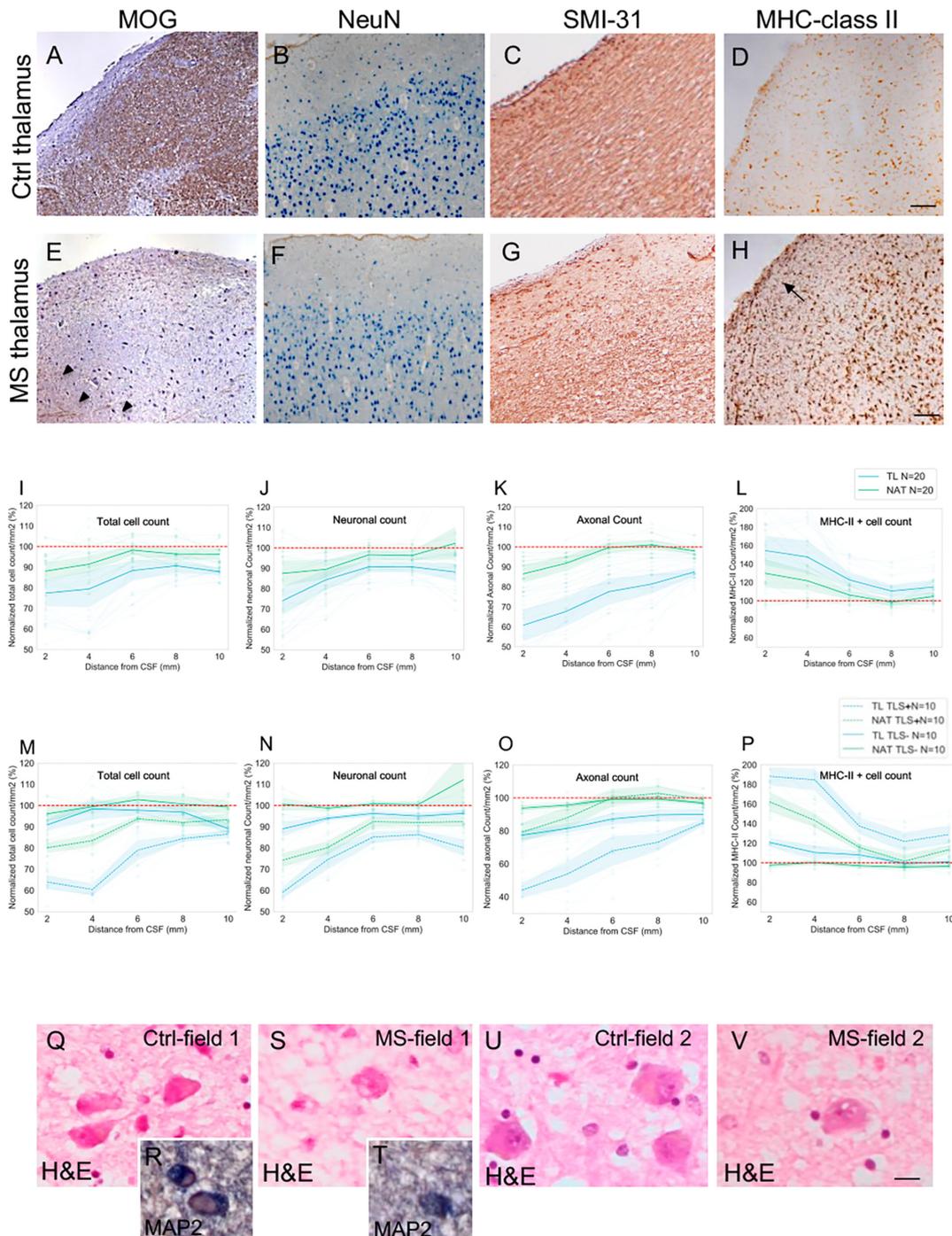
FIGURE 2: Neuropathological characterization of thalamic lesions in MS compared to non-neurological control: immunohistochemical detection of myelin oligodendrocyte glycoprotein (MOG; A, E), neuronal nuclei (NeuN; B, F), and axons (SMI31, C, G) and major histocompatibility complex class II molecules (MHC-II; D, H) in postmortem thalamic medial nuclei from age matched healthy control (A–D) and SPMS (E–H) cases. Demyelination (underlined by arrowheads) was observed in subependymal thalamic cortical area of MS case (E) but not in individuals without any neurological conditions, control (Ctrl; A). Reduction in number of NeuN^{+} neuronal cells (F) and SMI31^{+} axons (G) axons was observed in the superficial periventricular portion of thalamic MS lesions but not in correspondent controls (B, C). Substantial increase in the density of MHC-II[+] microglia/ macrophages was detected in the same areas close to the ependymal/CSF boundary (arrows) of thalamic lesion (H) of an SPMS case. Quantitative analysis of total cell counts (I, M), NeuN^{+} neurons (J, N), SMI-31 axons (K, O) and MHC class II[+] microglia/ macrophages (L, P) in thalamic lesions (TL; blue line) and in normal appearing thalamus (NAT; green line) of 20 postmortem MS cases and 5 non-neurological controls within 5 consecutive fields of view (20× objective), moving from the CSF-thalamic interface toward the internal capsule for a distance of 10 mm from the CSF/ependyma boundary. All graphs report mean cell counts (density expressed as number of cells/mm$^2$) normalized with respect to the cell counts in the controls, according to the distance from CSF. Shaded areas represent 95% confidence intervals. Graphs M-P report the cell density changes in MS brains stratified according to the presence (TLS[+], dashed lines) or absence (TLS[−], solid lines) of meningeal TLS. (Q–V) Morphological analysis of hematoxylin-eosin staining or MAP2 immunostaining (insets R, T) describes enlargement and rounding of neuronal cell body, peripheral localization of the nucleus and enlargement of the nucleolus in MS (IS, inset T, V) respect to controls (Q, inset R, U) in the external fields 1 and 2 of the thalamic lesions. Scale bar: 500 μm (A–H), 20 μm (Q–V). CSF = cerebrospinal fluid; MHC = major histocompatibility complex; MS = multiple sclerosis; SPMS = secondary-progressive multiple sclerosis.

optimized procedures.[30] All CSF samples were run in duplicate in the same experiment and blinded to group condition. The complete list of the CSF levels (pg/ml) of each molecule analyzed is reported in Appendix S1.

### Descriptive Analysis and Statistical Modeling
Descriptive statistics were expressed as mean ± standard error mean or median (interquartile range [IQR]). Differences between the 2 groups were evaluated using the unpaired Mann–Whitney test and Fisher's exact test. Spearman correlation was used to test for statistically significant correlation between groups (eg, between the relative changes of microglia density and neuronal/axonal changes) and the Spearman $R$- and $p$ values reported in each instance and graph. Statistical significance was considered when $p < 0.05$. Statistical analysis and graphing were performed using GraphPad Prism (version 8.0; GraphPad).

We modeled the gradient of cell count abnormalities with distance from CSF using mixed effects models of the form:

$$normalizedCount = \beta_0 + \beta_1 \cdot field + \beta_2 \cdot follicle +$$
$$\beta_3 \cdot tissue + \beta_4 \cdot distance \cdot follicle + \beta_5 \cdot distance \cdot tissue +$$
$$\beta_6 \cdot follicle \cdot tissue + \beta_7 \cdot distance \cdot follicle \cdot tissue + \gamma_{subject} + \epsilon.$$

where *normalized count* was the MHCII$^+$, neuron, or total cell count divided by the mean count from controls in the corresponding field; *field* was the microscopic field from which the count originated (ranging from 1, nearest the CSF interface, to 5, farthest away); *follicle* was 0 for TLS$^-$ and 1 for TLS$^+$; *tissue* was 0 for NAT and 1 for TL. The random effect $\gamma_{subject}$ was a subject-specific intercept and $\epsilon$ the residual error.

To assess the correlation between concentration of CSF molecules and cell counts, we applied a similar mixed effect model with replacement of the "follicle" term with "molecule," which was the concentration of the specified molecule in CSF. Marginal $R^2$ ($R_m^2$) and conditional $R^2$ ($R_c^2$) were computed, indicating the proportion of variance explained by the fixed effects, and by the fixed plus random effects, respectively.[31] Data processing and analysis was performed using the lme4 package[32] in R (version 4.0.2) and additional data processing and statistical software (ShadowLab Research) written in Python (version 3.6.2).

## Results
### Frequency and Characteristics of Demyelination
Demyelination in the dorsomedial nucleus of the thalamus was detected in 37 out of the 41 MS cases (90.24%); see Table S1, Fig 1A–C, Fig 2E), but in none of the non-inflammatory neurodegenerative cases, such as dementia with Lewy bodies (see Fig 1D), Alzheimer's disease, Parkinson's disease, or other neurological diseases, such as ischemic encephalopathy (see Fig 1E), HIV encephalitis (see Fig 1F), and MOGAD (see Fig 1G), or the non-neurological controls (see Fig 2A). Specifically, 15 out of the 37 TLs were classified as active demyelinating lesions (ALs; 40.55%), 13 as chronic active lesions (CALs; 35.13%), and 9 as inactive lesions (IALs; 24.32%; see Table S1). The presence of an AL was significantly associated with early age at onset (mean = 27.21 ± 4.28 vs mean: 35.16 ± 6.88; $p$ = 0.001), shorter disease duration (19.21 ± 6.05 vs 30.48 ± 12.78; $p$ = 0.0052), and early age at death (46.43 ± 7.67 vs 65.46 ± 9.68; $p$ = 0.0001), compared to the presence of CAL and IAL.

### Qualitative and Quantitative Assessment of Gradient of Thalamic Neuropathology
Qualitative investigation of neuropathology features of lesions in dorsomedial nucleus of the thalamus (see Figs 1C, H, 2A, E) of a selected group of 20 MS and 5 non-neurological control cases, previously analyzed for the "surface-in" gradient of subpial cortical damage,[3] revealed increased density of MHC-II$^+$ microglia/macrophages close to the CSF/ependyma boundary in MS cases with active thalamic demyelination (see Figs 1H, 2H) compared to both neurological (see Fig 1H–L) and non-neurologic controls (see Fig 2D). Only rare and scattered MHC-II$^+$ activated microglial cells were identified in other inflammatory neurological disease thalamic tissue samples in the subependymal area, with the majority of microglia/macrophages detected as discreet foci adjacent to parenchymal vessels (see Fig 1J–L). Parallel reduction in the density of NeuN$^+$ neurons (see Fig 2F) and SMI31$^+$ stained axons (see Fig 2G) was observed in the same subependymal TLs in comparison to controls (see Fig 2B, C).

Quantitative analysis of cell counts in the thalamus from the 20 MS brains, stratified according to the presence/absence of meningeal TLS (10 with and 10 without meningeal TLS), and 5 non-neurological controls demonstrated: significant reduction in total cell density in TLs (26%; $p$ = 0.0001) and in NAT (12%; $p$ = 0.0003); reduction of total number of NeuN$^+$ neurons in TL (19%; $p$ = 0.0001) and in NAT (11%; $p$ = 0.0005); reduction of total SMI31$^+$ axons in TL (23%; $p$ = 0.002) and in NAT (10%; $p$ = 0.004); increase in total MHC class II activated microglia/macrophages in TL (55%; $p$ = 0.0001) and in NAT (29%; $p$ = 0.0003), all with respect to controls.

When cell counts were measured in MS TLs according to the distance from the CSF surface, a gradient of cell loss was found, highest close to the ventricular

surface (mean reduction 23 ± 15%, standard error mean) and decreasing up to 10 mm inward (mean reduction 12 ± 4%), with respect to control (see Fig 2I). In particular, neuronal densities were decreased by 26 ± 16% at 2 mm from the thalamic ventricular surface and by 12 ± 10% at 10 mm (see Fig 2J). Similarly, graded reduction in SMI31$^+$ axon density was observed in MS TLs compared with controls, greatest (38 ± 12%) at 2 mm from the ependyma/CSF boundary and least with increasing distance (13 + 11%) at 10 mm (see Fig 2K). This gradient was reversed for activated (MHC-II$^+$) microglia/macrophages, quantified as an increase of 55 ± 36% at 2 mm from the thalamic ventricular surface up to 15 ± 17% at 10 mm from the ventricular surface (see Fig 2L). In MS NAT regions, a similar gradient of total cell loss was found that was highest close to the ventricular surface (12 ± 9% reduction) with respect to the more internal areas (4 ± 6% reduction; see Fig 2I). Neuron densities were significantly decreased by 13 ± 14% at 2 mm from the ventricular surface and nonsignificantly increased by 2 ± 18% at 10 mm (see Fig 2J). Similar significant decreased axon density was observed only at 2 mm from the ependyma (12 ± 10%; see Fig 2K). On the contrary, the density of activated (MHC-II$^+$) microglia/macrophages were significantly increased at 2 mm from CSF surface (30 ± 35%) and decreasing to 5 ± 10% at 10 mm from the CSF surface (see Fig 2L).

### The Gradient of Thalamic Pathology Is Greater in Cases Characterized by Tertiary Lymphoid-Like Structures

When secondary-progressive multiple sclerosis (SPMS) cases were stratified according to the presence or absence of meningeal inflammation, more pronounced cell changes were observed in TLS + MS cases with respect to TLS-MS (see Fig 2M). The highest reduction in neuron density with respect to controls was observed in TLs (41 ± 4%) and normal-appearing GM (NAGM; 26 ± 5%) of TLS + MS cases in comparison to TL (11 ± 6%) and NAT (1 ± 5% increase) of TLS-SPMS cases at 2 mm from CSF surface (see Fig 2N). Similarly, highest reduction in axon density with respect to controls was observed in TL (52 ± 9%) and NAGM (21 ± 8%) of TLS + MS cases in comparison to TL (22 ± 9%) and NAT (4 ± 3% increase) of TLS-SPMS cases at 2 mm from CSF surface (see Fig 2O). The largest increase in microglial density was observed in TL (88 ± 15%) and NAT (62 ± 16%) of TLS + MS cases in comparison to TL (21 ± 7%) and NAT (2 ± 3% decrease) of TLS-MS cases at 2 mm from CSF surface (see Fig 2P).

As reported in detail in the Supplementary Material, the results of mixed effect models fitted to the cell counts confirmed the presence of significantly steeper slopes (indicating greater cell abnormalities in proximity to the ventricular interface) in TLS$^+$ versus TLS$^-$ participants (total cells: 2.5 ± 0.78%, $p = 0.0014$; neurons: 2.3 ± 1.0%, $p = 0.026$; MHC-II$^+$: −13 ± 1.8%, $p < 0.0001$).

In addition to neuronal cell loss, morphometric analysis of MAP2$^+$ neuronal cell shape and morphology revealed significant increase in neuronal f-circle (cell circularity) only in the most external fields 1 ($p = 0.027$) and 2 ($p = 0.016$), up to 6 mm from the CSF/ependyma boundary, in the TLs of TLS + MS cases, but not in TLS-MS ones, with respect to controls (see Fig 2 insets R, T; Table 2). Combined analysis of hematoxylin-eosin staining confirmed enlargement and rounding of neuronal cell body, peripheral localization of the nucleus, and enlargement of the nucleolus in MS with respect to controls (see Fig 2Q–V) in the same external portion of the TLs (Fig 3).

### Specific CSF Inflammatory Protein Levels Associate with the Gradient of Thalamic Pathology

We then assessed the relationship between the concentration of markers of inflammation and axonal damage in the CSF and the gradient of cell counts in the same individuals (Table 3). We observed an inverse correlation ($p < 0.001$) between the neuronal count in proximity to the ventricular surface (intercept) and the CSF levels of several inflammatory markers, including chitinase-3-L1, parvalbumin, sTNFR1, Nf-L, TNF, fibrinogen, and IFN-γ (see Table 3). Interestingly, most of these molecules showed a significant positive correlation with the slope of the trajectory of neuronal cell counts as a function of the distance from the CSF, hence correlating with the greater decrease in neuronal counts moving from the thalamic inner fields toward the ventricular ones (see Table 3).

The concentration of several CSF molecules also showed significant ($p < 0.001$) positive correlations with the MHC-II cell count on the thalamic ventricular side (intercept): these included Nf-L, chitinase-3-L1, parvalbumin, CCL21, sTNFR1, TNF, CCL19, CCL22, CXCL10, CXCL13, and IFN-γ. A significant correlation ($p < 0.05$) was also observed for sCD163, fibrinogen, IL2, IL10, osteopontin, and BAFF. These molecules also showed a negative correlation with the slope of MHC-II counts from the superficial to the inner portions of the thalamus, indicating that their increase was associated with a steeper gradient of MHC-II cell abnormalities (see Table 3).

| | Controls | TL TLS$^+$ | NAT TLS$^+$ | TL TLS$^-$ | NAT TLS$^-$ |
| Field | Mean (SD) | Mean (SD) | Mean (SD) | Mean (SD) | Mean (SD) |
|---|---|---|---|---|---|
| 1 | 0.733 (0.03) | 0.782 (0.05)* | 0.752 (0.04) | 0.755 (0.05) | 0.746 (0.04) |
| 2 | 0.758 (0.04) | 0.798 (0.03)* | 0.771 (0.04) | 0.770 (0.03) | 0.762 (0.06) |
| 3 | 0.784 (0.07) | 0.801 (0.04) | 0.795 (0.03) | 0.773 (0.04) | 0.787 (0.05) |
| 4 | 0.792 (0.04) | 0.809 (0.03) | 0.797 (0.06) | 0.796 (0.04) | 0.791 (0.03) |
| 5 | 0.756 (0.06) | 0.769 (0.03) | 0.761 (0.04) | 0.762 (0.05) | 0.761 (0.05) |

**TABLE 2. Measures of Neuronal f-Circle**

* indicates significant change ($p < 0.05$) compared to controls. NAT = normal appearing thalamus; TL = thalamic lesion; TLS = tertiary lymphoid-like structure.

For most of these molecules, there was no significant difference in their correlation with the neuronal and MHC-II$^+$ cell counts in TLs or NAT. The only exceptions were CCL19, which was associated with a modest additional decrease in neuronal count in TL ($-0.0150$, $p < 0.05$), and fibrinogen, which was associated with further increase in MHC-II$^+$ count in TL ($+2.310$, $p < 0.05$). The complete list of molecules tested, the mixed effect models' estimates, $R^2$, and $p$ values are reported in the Supplementary Material.

### Characterization of the Microglial Phenotype in Thalamic Lesions

Spearman correlation analysis revealed significant correlation between microglia density with neuronal density either at the most external measured area close to the CSF/ependyma (R = $-0.91$, $p < 0.0001$; Fig 3A) and at the most internal area (8 mm; R = $-0.84$, $p < 0.0001$; Fig 3B). Similar correlation was found between microglia density and axonal density at the CSF/ependyma boundary (R = $-0.79$, $p < 0.0001$; Fig 3C) and, less at the most internal area (R = $-0.32$, p: 0.042; Fig 3D). Immunohistochemical characterization of the microglia/macrophage markers expressed in the active TL (see Fig 3E, inset F) of the examined MS cases revealed that MHC-II$^+$ microglia in the most external fields 1 and 2, close to the CSF surface, mainly expressed TMEM119 (mean percentage = 72%; see Fig 3G, H) and in smaller proportion the marker of antigen presentation CD11c (mean percentage = 56%; see Fig 3I). Only limited numbers of CD68$^+$ microglia/macrophages (see Fig 4E) and P2Ry12$^+$ resting resident microglia (see Fig 3J, K) were observed in the same portions of the lesions. On the contrary, macrophages expressing CD68, CD86, or CD163 (see Fig 3L–N) were detected in the Virchow-Robin space of large subependymal infiltrates within the TLs.

### Characterization of Subependymal Infiltrates in Thalamic Lesions Revealed an Increase in B-Cell Numbers

In addition to an elevated number of macrophages, large perivascular subependymal infiltrates within TLs (Fig 4A) included a variable number of scattered CD3$^+$ T-cells (Fig 4B, F, J), elevated numbers of CD20$^+$ B cells, which often occurred as aggregates (see Fig 4C, G, K) and scattered Ig-expressing plasma cells (see Fig 4D, H). In addition, CD35$^+$ follicular dendritic cells were observed within the Virchow-Robin of the subependymal infiltrates of 5 out of the 10 TLS + MS cases (see Fig 4E, I, L), but not in TLS-MS. The expression of CXCL13 was detected in some of the B-cell enriched subependymal infiltrates (see Fig 4M). The presence of such large subependymal infiltrates was a major characteristic of TLS$^+$ MS cases (7 out of the 10 examined), whereas only a minor fraction of TLS$^-$ cases (2 out of the 10 examined) presenting similar large (diameter = 200–500 μm) subependymal infiltrates (see Fig 4N). The number of CD3$^+$ T-cells (mean = $31.1 \pm 13.5$; range = 15–54) and CD20$^+$ B-cells (mean = $73.5 \pm 11.7$; range = 34–120) per subependymal infiltrate per case demonstrated a substantially increased proportion of B-cells in TLS$^+$ MS cases (see Fig 4O).

### Discussion

Neuropathological, clinical, and imaging evidence has demonstrated a significant involvement of the thalamus from the earliest stages of MS,[23,24] and greater volume loss, as compared to cortical and deep GM, in subjects with clinically and radiologically isolated syndromes.[33,34] In our study, we report that the presence of active inflammatory demyelinating TLs, observed in 40% of the cohort of postmortem progressive MS cases, was associated with a younger age at onset, a more rapid and severe disease
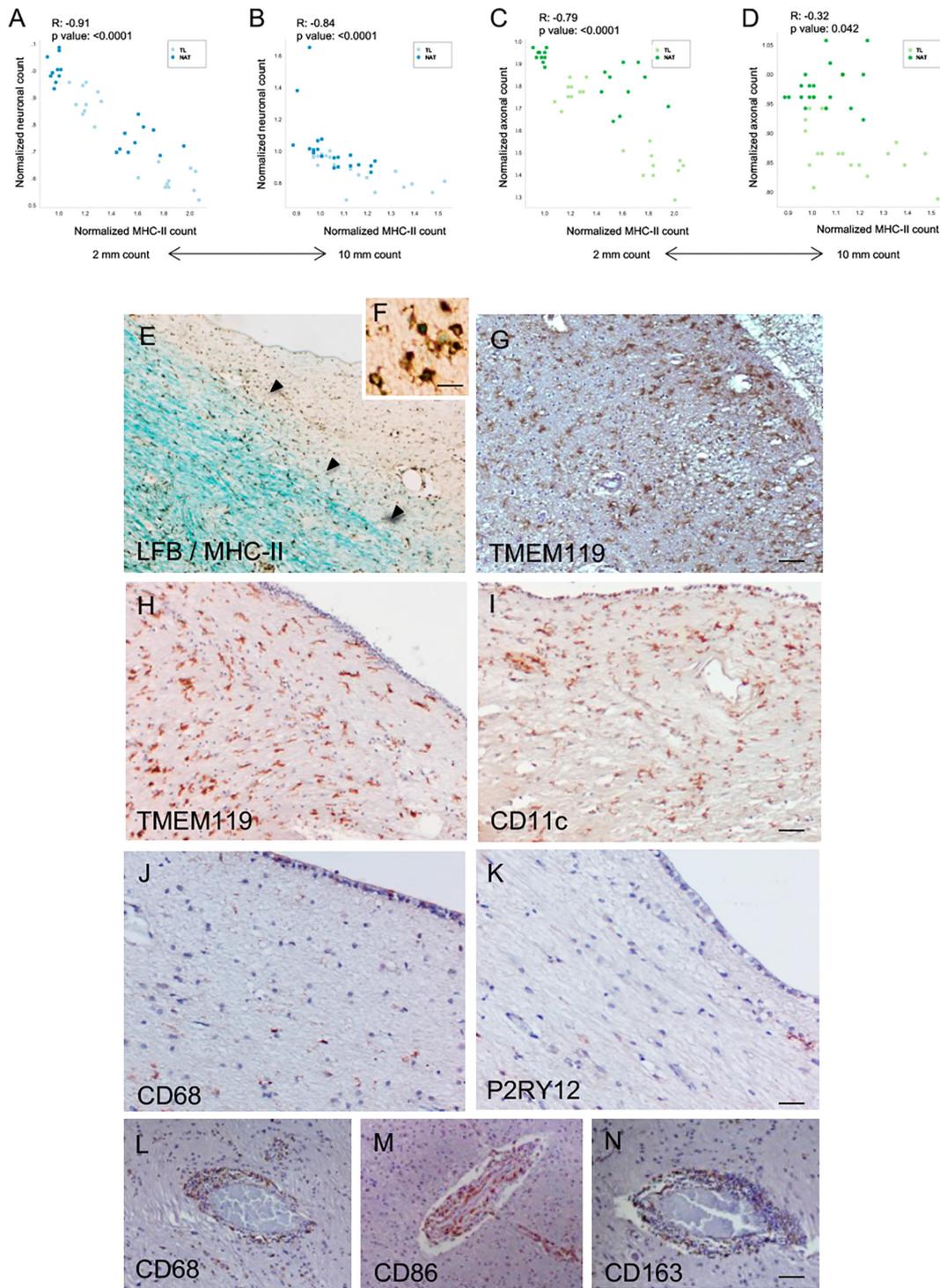
FIGURE 3: Spearman correlation analysis between microglia density (density expressed as number of cells/mm² and normalized with respect to the cell counts in the controls) and neuron density (A, B) Normalized respect to microglia density measured in the controls) or axon density (C, D) normalized respect to microglia density measured in the controls). Graphs report the correlation analysis at the most external measured area close to the CSF/ependyma boundary, 2 mm, (A, C) and at the most internal area (8 mm, B, D). Spearman correlation index R and *p* value is reported for each graph. (E–Q) Neuropathological characterization of microglial activation in thalamic lesions. Active thalamic demyelination (E, inset F) was revealed by the immunostaining of major histocompatibility complex class II molecule (MHC-II) combined with the myelin staining Luxol Fast Blue (LFB). Abundant presence of TMEM119⁺ microglia was evident in the parenchyma of thalamic lesions particularly close to the ependymal/CSF boundary (G, H), where concomitant expression of the antigen presentation marker CD11 was also observed (I). Only a limited number of CD68⁺ microglia/macrophages (J) and P2Ry12⁺ resting resident microglia (K) were observed in the same external portions of the lesions. On the contrary, the Virchow-Robin space of subependymal vessels observed in active thalamic lesions contained macrophages mainly expressing CD68 (L), CD86 (M) or CD163 (N). Scale bars: μm (L–N), 500 μm (E–K), 20 μm (inset F). CSF = cerebrospinal fluid; MOG = myelin oligodendrocyte glycoprotein; MS = multiple sclerosis; TLS = lymphoid-like structure.

**TABLE 3. List of the CSF Molecules Correlating with Gradient of Normalized Neuronal and MHC-II Cells Counts**

| CSF molecule | Intercept NAT | Slope NAT | Intercept TL | Slope TL |
|---|---|---|---|---|
| | Neuronal cell counts | | | |
| Chitinase-3-like-1 | -1.2674e-03 | 1.0091e-04 | -1.6604e-03 | 2.3765e-04 |
| sTNF-R1 | −6.0639e-03 | 8.9050e-04 | -6.4063e-03 | 8.6601e-04 |
| PVALB | −4.5302e-01 | 7.4909e-02 | −4.7689e-01 | 7.4905e-02 |
| NfL | −1.9941e-01 | 1.8342e-02 | −2.6173e-01 | 3.4811e-02 |
| TNF-alpha | −2.3651e+00 | 3.1561e-01 | −2.7172e+00 | 4.3264e-01 |
| sCD163 | −4.6058e-05 | 4.6066e-06 | −6.6890e-05 | 1.0671e-05 |
| CCL21 | −7.5644e-03 | 4.7281e-04 | −1.1328e-02 | 1.5520e-03 |
| Fibrinogen | −1.3619e+00 | 1.9618e-01 | −1.5779e+00 | 2.5801e-01 |
| CCL19 | −1.8801e-02* | 1.4673e-03 | −3.3764e-02* | 5.5991e-03 |
| IL-2 | −6.9683e-01 | 9.2707e-02 | −7.4687e-01 | 1.0183e-01 |
| BAFF | −1.6370e-03 | 3.0289e-04 | −1.2165e-03 | 1.3235e-04 |
| CXCL10 | −3.0348e-03 | 2.3338e-04 | −5.1040e-03 | 7.7514e-04 |
| IFN-γ | −1.0657e-01 | 1.2213e-03 | −1.7946e-01 | 2.5524e-02 |
| | MHC-II+ cell count | | | |
| NfL | 6.9119e-01 | −1.3191e-01 | 7.7885e-01 | −1.2949e-01 |
| Chitinase-3-like-1 | 3.8585e-03 | −7.1654e-04 | 3.7771e-03 | −4.6497e-04 |
| CCL21 | 2.6217e-02 | −5.0357e-03 | 3.2627e-02 | −5.0695e-03 |
| PVALB | 1.0088e+00 | −1.9494e-01 | 1.0787e+00 | −1.3730e-01 |
| sTNF-R1 | 1.3332e-02 | −2.4313e-03 | 1.7834e-02 | −2.6763e-03 |
| TNF-alpha | 5.6823e+00 | −1.1088e+00 | 6.8719e+00 | −9.8644e-01 |
| CCL19 | 6.4723e-02 | −1.2396e-02 | 8.0151e-02 | −1.3391e-02 |
| CCL22 | 1.0391e+00 | −2.0050e-01 | 1.1084e+00 | −1.4463e-01 |
| CXCL10 | 1.1324e-02 | −2.1216e-03 | 1.3160e-02 | −2.2257e-03 |
| CXCL13 | 1.0335e+00 | −2.0308e-01 | 1.2564e+00 | −1.8533e-01 |
| IFN-γ | 3.7935e-01 | −6.9188e-02 | 3.5126e-01 | −3.4123e-02 |
| sCD163 | 1.0791e-04 | −1.9157e-05 | 1.5372e-04 | −2.3121e-05 |
| Fibrinogen | 3.1042e+00* | −6.2587e-01 | 5.4140e+00* | −9.4240e-01 |
| IL-2 | 1.7682e+00 | −3.4171e-01 | 2.0161e+00 | −2.9482e-01 |
| IL-10 | 4.1074e+00 | −8.1181e-01 | 3.0764e+00 | −1.9105e-01 |
| IL-12-p70 | −8.6644e+01 | 1.6676e+01 | −1.0201e+02 | 1.7659e+01 |
| IL-5 | −6.4402e+01 | 1.2815e+01 | −7.0779e+01 | 1.0996e+01 |
| Osteopontin | 1.9276e-03 | −3.7657e-04 | 2.3841e-03 | −3.9523e-04 |
| BAFF | 3.7817e-03 | −7.2672e-04 | 4.5562e-03 | −7.3216e-04 |

Correlation of CSF molecules with gradient of normalized neuronal and MHC-II cells counts. The table report the CSF molecules showing significant correlations with the intercept (indicating the cell count in closest proximity to the ventricular interface) and the slope of the gradient of neuronal (A) and MHC-II cells (B) densities. Red and blue colors indicate significant positive and negative estimates, respectively, with darker colors indicating significance of $p < 0.001$, and lighter colors of $p < 0.05$.

CSF = cerebrospinal fluid; NAT = normal appearing thalamus; PVALB = parvalbumin; TL = thalamic lesion.
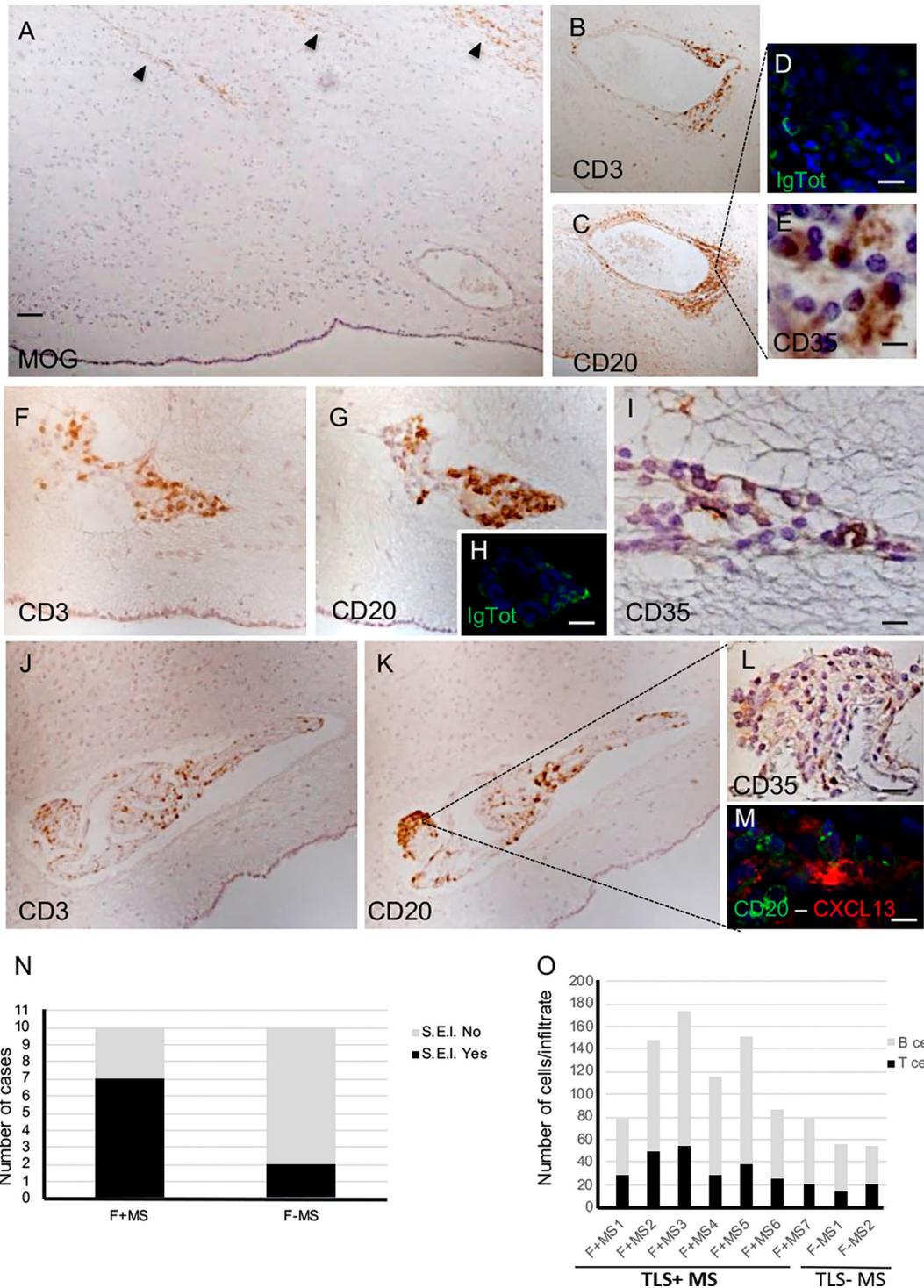
FIGURE 4: Neuropathological characterization of subependymal perivascular infiltrates (SEIs) in thalamic lesions. Numerous, large perivascular inflammatory infiltrates are detected in thalamic MS lesions (A, underlined by arrowheads) in close proximity to the ependyma (A, B, C, F, G, I, J, K). These infiltrates contained a variable number of scattered CD3$^+$ T cells (B, F, J) and an elevated number of CD20$^+$ B cells (C, G, K), often aggregated in a compact cluster. Within the B-cell enriched portion of the subependymal infiltrates, CD35$^+$ follicular dendritic cells (FDCs) were also found (E, I, L), in combination with the expression of CXCL13 (M) and the presence of a substantial number of Ig-producing plasma cells (D, H). Scale bars: 1000 μm (A), 200 μm (B, C, F, G, J, K, L); and 20 μm (D, E, H, M). The frequency of large SEIs in TLS$^+$ SPMS cases (7 out of the 10 examined) and in TLS-SPMS cases (2 out of the 10 examined) are reported in graph N; the number of CD3$^+$ T cells and CD20$^+$ B cells for each of the detected large SEI in TLS$^+$ and TLS$^-$ SPMS examined cases are reported in graph O. MHC = major histocompatibility complex; MOGAD = myelin oligodendrocyte glycoprotein-antibody-associated disease; MS = multiple sclerosis; SPMS = secondary-progressive multiple sclerosis; TLS = lymphoid-like structure.

course, shorter disease duration, and younger age at death compared to MS cases with chronic active or inactive TLs. Surprisingly, a substantial proportion of TLs detected in our study (40%) were still active at time of death, mainly at the level of the CSF-ependymal boundary, despite a mean disease duration of 25 years. Whereas previous neuropathology studies have reported a very low frequency of active lesions in patients with chronic MS,[35] our findings further support the hypothesis that lesion activity and inflammation may persist throughout disease progression, at least in a subgroup of chronic MS cases with more rapid and severe progression. In addition, we revealed that thalamic MS pathology occurs according to a "surface-in" gradient from the CSF-ependymal boundary into the deep GM and includes neuronal and axonal loss and morphological neurodegenerative changes, accompanied by a substantial increase in microglial density. This is in agreement with recent data obtained from both MRI and PET imaging studies[17–20,36–38] even at early stages in pediatric patients with MS.[23,24,33] In particular, this "ependymal-in" pattern of injury appears to occur independently of demyelination and is higher in MS brains with increased inflammation, either in the meninges (TLS[+]) or as large subependymal infiltrates.

A surface-in gradient of cortical damage, in particular subpial, has been described in postmortem MS cases and suggested as an important pathologic substrate of clinical progression in MS.[3,17] Increasing evidence supports a relationship between periventricular and subpial abnormalities.[20] Despite being suggested to be linked to progressive disease biology, the abnormalities at the brain/CSF interfaces are already seen early in the course of pediatric and adult-onset MS.[20,23,24,33] The gradient of damage in the thalamus, like that in the cortical layers, appears to be substantially influenced and intensified by the presence of meningeal TLS enriched in B-cells, suggesting that intrathecal inflammation may play a crucial role in prevalence of MS lesion distribution in the outermost subpial and subependymal (periventricular) GM regions and in exacerbating neurodegeneration, either directly or indirectly by releasing inflammatory and/or cytotoxic factors into the CSF.[8–14,39–42] Interestingly, our data showing that the graded thalamic injury persists up to the time of death, in the presence of diffuse microglial activation and perivascular inflammatory infiltrates, support the hypothesis that chronic inflammation persists throughout the disease course.[42,43]

The strong association of thalamic pathology with the presence of cortical meningeal ectopic TLS, enriched in B cells, further substantiates the hypothesis that meningeal lymphoid-neogenesis and increased intrathecal inflammation have a fundamental role, not only in subpial GM

pathology but also in the deep GM. Inflammatory/cytotoxic factors produced by meningeal infiltrates, possibly related to the elevated B cell activity and released into the CSF, could cause damage not only to the regions adjacent to the meningeal TLS, but also diffusely across all the brain[20] and spinal cord[44,45] surfaces. It was previously suggested that B cells from patients with MS but not controls, in addition to secretion of pro-inflammatory molecules, such as TNF, lymphotoxin-α, IL-6, and GM-CSF, may also secrete one or more factors toxic to oligodendrocytes and neurons that can possibly directly contribute to demyelination in patients with MS.[8–11,16,44–46] Here, we indeed found that, among a large panel of inflammatory mediators examined in the CSF from the same MS cases used for thalamic cell counts, only a specific subgroup of molecules related to both innate immune activity and lymphoid neogenesis (CCL19, CXCL10, and CXCL13) and major inflammatory factors (including sTNFR1, fibrinogen, IFN-γ, IL-2, and IL-10), strongly associated with the gradient of increased microglial density in the thalamus of progressive MS cases. As previously suggested,[16] CSF levels of TNF and its pro-inflammatory soluble receptor, sTNFR1, appear to represent good surrogate correlates of the "surface-in" GM pathology. In addition, CSF levels of markers of neurodegeneration, such as neurofilament light-chains and parvalbumin (PVALB), were found correlated with neuronal loss in the thalamus. CSF parvalbumin, a GABAergic neuronal marker recently found associated with GM atrophy,[30] showed the highest correlation with neuronal loss when compared to NfL levels, supporting the idea that this molecule may represent a potential MS-specific biomarker of neuronal injury. All the correlations were also characterized by a slope reflecting steeper changes with increasing distance away from the ventricular surface, in agreement with the idea that CSF inflammatory/cytotoxic factors may induce diffuse pathological cell alterations directly, by mediating neuroaxonal injury, and/or indirectly, by activating tissue resident microglia and astrocytes. The observed significant association observed in MS TLs between gradient of microglia activation and gradient of neuro-axonal decreased density strongly support this hypothesis. Moreover, this idea is supported by a recent longitudinal, prospective study of patients with relapsing–remitting MS at the time of diagnosis showing that CXCL13 and sCD163 CSF protein levels were independent predictors of thalamic ($R^2$ model $= 0.80$; $p < 0.001$) and hippocampal ($R^2$ model $= 0.47$; $p < 0.001$) volume change after 2-year follow-up.[46] In addition, chronically elevated TNF and IFN-γ cytokine concentrations in the CSF in vivo in a rat model have been demonstrated able to induce microglial activation, subpial demyelination, and neuronal loss in the

cortical layers underlying the subarachnoid space.[12,15] These data strongly suggest a key role of intrathecal inflammation in the slow build-up of diffuse GM pathology, in particular, in neuronal loss and aberrant rounding morphology, that as previously shown may be mediated by TNF/TNFR1-mediated necroptosis (rather than apoptosis), possibly related to chronic meningeal inflammation.[47]

The "surface-in" gradient and the correlation with CSF inflammation were found in both active TLs and NAT, indicating that microglial activation and neuroaxonal degeneration are likely to be partially independent of myelin loss, as has also been shown in cortical GM.[1,3,47,48] Pathological changes in NAT were particularly evident in MS brains with elevated meningeal inflammation, but not in MS brains without, which showed measures of cell density similar to non-neurological controls. These findings strongly support a key role of intrathecal inflammation in the slow build-up of diffuse pathology and may have important clinical implications possibly explaining long-term MS worsening, independent of relapse activity, also known as "silent disease activity."[49]

We found an elevated presence of immune perivascular infiltrates in periventricular large veins in the active TLs. These veins are found close to the ependymal surface and drain toward the periventricular surface. Perivascular spaces have been shown to increase in size and number in MS brains[50] and this event may also influence the inflammatory conditions. Interestingly, we found that the inflammatory infiltrates in active TLs were particularly rich in CD20$^+$ B cells, often closely aggregated and accompanied by the presence of CD35$^+$ follicular dendritic cells (FDCs), particularly in MS cases also characterized by the presence of TLS in the meninges. This suggests that the accumulation of inflammatory cells in the Virchow-Robyn spaces, which are characterized by increased amounts of connective tissue, may contribute to the persistence of compartmentalized intracerebral inflammation and, in turn, to disease exacerbation in the deep GM.[51–54] Our data give an insight into the central nervous system (CNS)-wide extent of compartmentalized inflammation that can possibly occur both in the leptomeningeal and in the brain perivenular infiltrates, possibly in a proportion of MS cases with increased B cell involvement, indicating one of the rationales of the success of existing and new anti-B cell treatments. In support of this, related B-cell clones have been previously found in both the cerebral meningeal and in parenchymal perivascular infiltrates.[55]

This study is not without limitations, including the lack of larger and independent cohorts of postmortem MS and control (other neurological conditions) groups, as well as the assessment of further components of tissue alterations. In addition, more in-depth assessment and understanding of the exact molecular mechanisms involved in surface-in pathology in progressive MS still need to be achieved.

## Conclusions

Thalamic pathology is a relatively common feature of progressive MS and we have shown that it follows a "surface-in" gradient of neuronal and axonal loss and microglial activation from the CSF/ependymal boundary toward the deep GM. In a specific MS subgroup, characterized by more rapid and severe disease progression, the extent of the gradients correlated with the presence of compartmentalized inflammation within meningeal TLS structures and large subependymal perivascular lymphoid-like infiltrates, both enriched in B cells, and with elevated level of CSF inflammation. These data support a key role for intrathecal B-cell immunity in MS-specific brain superficial cortical and periventricular injury, possibly related to intrathecally compartmentalized inflammation and to a specific disease endophenotype. CSF biomarkers, together with advanced imaging tools, may therefore help to improve not only the disease diagnosis but also the early identification and stratification of specific MS subgroups that would benefit with more personalized treatments.

Additional work will be needed to determine the exact molecular functions/mechanisms involved in the "surface-in" damage in MS that could be targeted by future MS therapies.

## Author Contributions

R.M., S.M., and R.R. contributed to the conception and design of the study. R.M., G.F., R.B., O.H., S.H., and R.N. contributed to the acquisition and analysis of data. R.M., A.B.O., O.W.H., S.H., D.M., A.P., R.N., M.C.,

S.M., and R.R. contributed to drafting and revision of the manuscript.

## Potential Conflicts of Interest

The authors declare no conflicts of interest related to this study.

## References

1. Peterson JW, Bö L, Mörk S, et al. Transected neurites, apoptotic neurons, and reduced inflammation in cortical multiple sclerosis lesions. Ann Neurol 2001;50:389–400.

2. Vercellino M, Masera S, Lorenzatti M, et al. Demyelination, inflammation, and neurodegeneration in multiple sclerosis deep gray matter. J Neuropathol Exp Neurol 2009;68:489–502.

3. Magliozzi R, Howell OW, Reeves C, et al. A gradient of neuronal loss and meningeal inflammation in multiple sclerosis. Ann Neurol 2010;68:477–493.

4. Magliozzi R, Howell OW, Vora A, et al. Meningeal B-cell follicles in secondary progressive multiple sclerosis associate with early onset of disease and severe cortical pathology. Brain 2007;130:1089–1104.

5. Howell OW, Reeves CA, Nicholas R, et al. Meningeal inflammation is widespread and linked to cortical pathology in multiple sclerosis. Brain 2011;134:2755–2771.

6. Haider L, Zrzavy T, Hametner S, et al. The topograpy of demyelination and neurodegeneration in the multiple sclerosis brain. Brain 2016;139:807–815.

7. Magliozzi R, Howell OW, Nicholas R, et al. Inflammatory intrathecal profiles and cortical damage in multiple sclerosis. Ann Neurol 2018;83:739–755.

8. Alcázar A, Regidor I, Masjuan J, et al. Axonal damage induced by cerebrospinal fluid from patients with relapsing-remitting multiple sclerosis. J Neuroimmunol 2000;104:58–67.

9. Lisak RP, Benjamins JA, Nedelkoska L, et al. Secretory products of multiple sclerosis B cells are cytotoxic to oligodendroglia in vitro. J Neuroimmunol 2012;246:85–95.

10. Duddy M, Niino M, Adatia F, et al. Distinct effector cytokine profiles of memory and naive human B cell subsets and implication in multiple sclerosis. J Immunol 2007;178:6092–6099.

11. Li R, Rezk A, Miyazaki Y, et al. Proinflammatory GM-CSF-producing B cells in multiple sclerosis and B cell depletion therapy. Sci Transl Med 2015;7:310ra166.10.

12. Gardner C, Magliozzi R, Durrenberger PF, et al. Cortical grey matter demyelination can be induced by elevated pro-inflammatory cytokines in the subarachnoid space of MOG-immunized rats. Brain 2013;136:3596–3608.

13. Vidaurre OG, Haines JD, Katz Sand I, et al. Cerebrospinal fluid ceramides from patients with multiple sclerosis impair neuronal bioenergetics. Brain 2014;137:2271–2286.

14. Calabrese M, Magliozzi R, Ciccarelli O, et al. Exploring the origins of grey matter damage in multiple sclerosis. Nat Rev Neurosci 2015;16:147–158.

15. James RE, Schalks R, Browne E, et al. Persistent elevation of intrathecal pro-inflammatory cytokines leads to multiple sclerosis-like cortical demyelination and neurodegeneration. Acta Neuropathol Commun 2020;8:66.

16. Magliozzi R, Howell OW, Durrenberger P, et al. Meningeal inflammation changes the balance of TNF signalling in cortical grey matter in multiple sclerosis. J Neuroinflammation 2019a;16:259.

17. Mainero C, Louapre C, Govindarajan ST, et al. A gradient in cortical pathology in multiple sclerosis by in vivo quantitative 7 T imaging. Brain 2015;138:932–945.

18. Liu Z, Pardini M, Yaldizli O, et al. Magnetization transfer ratio measures in normal-appearing white matter show periventricular gradient abnormalities in multiple sclerosis. Brain 2015;138:1239–1246.

19. Brown JW, Pardini M, Brownlee WJ, et al. An abnormal periventricular magnetization transfer ratio gradient occurs early in multiple sclerosis. Brain 2017;140:387–398.

20. Pardini M, Brown JWL, Magliozzi R, et al. Surface-in pathology in multiple sclerosis: a new view on pathogenesis? Brain 2021;144:1646–1654.

21. Lucchinetti CF, Popescu BF, Bunyan RF, et al. Inflammatory cortical demyelination in early multiple sclerosis. N Engl J Med 2011;365:2188–2197.

22. Bevan RJ, Evans R, Griffiths L, et al. Meningeal inflammation and cortical demyelination in acute multiple sclerosis. Ann Neurol 2018;84:829–842.

23. Fadda G, Brown RA, Magliozzi R, et al. A surface-in gradient of thalamic damage evolves in pediatric multiple sclerosis. Ann Neurol 2019;85:340–351.

24. De Meo E, Storelli L, Moiola L, et al. In vivo gradients of thalamic damage in paediatric multiple sclerosis: a window into pathology. Brain 2021;144:186–197.

25. Cooze BJ, Dickerson M, Loganathan R, et al. The association between neurodegeneration and local complement activation in the thalamus to progressive multiple sclerosis outcome. Brain Pathol 2022;e13054.

26. Nicholas R, Magliozzi R, Campbell G, et al. Temporal lobe cortical pathology and inhibitory GABA interneuron cell loss are associated with seizures in multiple sclerosis. Mult Scler 2016;22:25–35.

27. Papadopoulos D, Dukes S, Patel R, et al. Substantial archaeocortical atrophy and neuronal loss in multiple sclerosis. Brain Pathol 2009;19:238–253. https://doi.org/10.1111/j.1750-3639.2008.00177.x.

28. Zrzavy T, Hametner S, Wimmer I, et al. Loss of 'homeostatic' microglia and patterns of their activation in active multiple sclerosis. Brain 2017;140:1900–1913.

29. Magliozzi R, Hametner S, Facchiano F, et al. Iron homeostasis, complement, and coagulation cascade as CSF signature of cortical lesions in early multiple sclerosis. Ann Clin Transl Neurol 2019b;6:2150–2163.

30. Magliozzi R, Pitteri M, Ziccardi S, et al. CSF parvalbumin levels reflect interneuron loss linked with cortical pathology in multiple sclerosis. Ann Clin Transl Neurol 2021 Jan 23;8:534–547.

31. Nakagawa S, Schielzeth H. A general and simple method for obtaining R2 from generalized linear mixed-effects models. Methods Ecol Evol 2013;4:133–142.

32. Bates D, Mächler M, Bolker B, Walker S. Fitting linear mixed-effects models using lme4. J Stat Softw 2015;67:1–48.

33. Mesaros S, Rocca MA, Absinta M, et al. Evidence of thalamic gray matter loss in pediatric multiple sclerosis. Neurology 2008;70:1107–1112.

34. Hidalgo de la Cruz M, Valsasina P, Mesaros S, et al. Clinical predictivity of thalamic sub-regional connectivity in clinically isolated syndrome: a 7-year study. Mol Psychiatry 2021 Jun;26:2163–2174.

35. Noseworthy JH, Lucchinetti C, Rodriguez M, Weinshenker BG. Multiple sclerosis. N Engl J Med 2000;343:938–952.

36. Poirion E, Tonietto M, Lejeune FX, et al. Structural and clinical correlates of a periventricular gradient of Neuroinflammation in multiple sclerosis. Neurology 2021;96:e1865–e1875.

37. Pardini M, Sudre CH, Prados F, et al. Relationship of grey and white matter abnormalities with distance from the surface of the brain in

multiple sclerosis. J Neurol Neurosurg Psychiatry 2016;87:1212–1217.

38. Jehna M, Pirpamer L, Khalil M, et al. Periventricular lesions correlate with cortical thinning in multiple sclerosis. Ann Neurol 2015;78:530–539.

39. Michel L, Touil H, Pikor NB, et al. B cells in the multiple sclerosis central nervous system: trafficking and contribution to CNS-compartmentalized inflammation. Front Immunol 2015;6:636.

40. Monaco S, Nicholas R, Reynolds R, Magliozzi R. Intrathecal inflammation in progressive multiple sclerosis. Int J Mol Sci 2020;21:8217.

41. Griffiths L, Reynolds ER, et al. Substantial subpial cortical demyelination in progressive multiple sclerosis: have we underestimated the extent of cortical pathology? Neuroimmunol Neuroinflam 2020;7:51–67.

42. Luchetti S, Fransen NL, van Eden CG, et al. Progressive multiple sclerosis patients show substantial lesion activity that correlates with clinical disease severity and sex: a retrospective autopsy cohort analysis. Acta Neuropathol 2018;135:511–528. https://doi.org/10.1007/s00401-018-1818-y.

43. Steinman L, Zamvil SS. Beginning of the end of two-stage theory purporting that inflammation then degeneration explains pathogenesis of progressive multiple sclerosis. Curr Opin Neurol 2016;29:340–344.

44. Reali C, Magliozzi R, Roncaroli F, et al. B cell rich meningeal inflammation associates with increased spinal cord pathology in multiple sclerosis. Brain Pathol 2020;30:779–793.

45. Ouellette R, Treaba CA, Granberg T, et al. 7 T imaging reveals a gradient in spinal cord lesion distribution in multiple sclerosis. Brain 2020;143:2973–2987.

46. Bajrami A, Magliozzi R, Pisani AI, et al. Volume changes of thalamus, hippocampus and cerebellum are associated with specific CSF profile in MS. Mult Scler 2021 Aug;11:13524585211031786.

47. Picon C, Jayaraman A, James R, et al. Neuron-specific activation of necroptosis signaling in multiple sclerosis cortical grey matter. Acta Neuropathol 2021;141:585–604.

48. Klaver R, Popescu V, Voorn P, et al. Neuronal and axonal loss in normal-appearing gray matter and subpial lesions in multiple sclerosis. J Neuropathol Exp Neurol 2015;74:453–458.

49. Cree BAC, Hollenbach JA, et al. Silent progression in disease activity-free relapsing multiple sclerosis. Ann Neurol 2019;85:653–666.

50. Wuerfel J, Haertle M, Waiczies H, et al. Perivascular spaces - MRI marker of inflammatory activity in the brain? Brain 2008;131:2332–2340.

51. Prineas JW. Multiple sclerosis: presence of lymphatic capillaries and lymphoid tissue in the brain and spinal cord. Science 1979;203:1123–1125.

52. Meinl E, Krumbholz M, Hohlfeld R. B lineage cells in the inflammatory central nervous system environment: migration, maintenance, local antibody production, and therapeutic modulation. Ann Neurol 2006;59:880–892.

53. Machado-Santos J, Saji E, Tröscher AR, et al. The compartmentalized inflammatory response in the multiple sclerosis brain is composed of tissue-resident CD8$^+$ T lymphocytes and B cells. Brain 2018;141:2066–2082.

54. Lovato L, Willis SN, Rodig SJ, et al. Related B cell clones populate the meninges and parenchyma of patients with multiple sclerosis. Brain 2011;134:534–541.

55. Comi G, Bar-Or A, Lassmann H, et al. Expert panel of the 27th annual meeting of the European Charcot Foundation. Role of B cells in multiple sclerosis and related disorders. Ann Neurol 2021;89:13–23.